MolecularMedicine

Nicotinic Acetylcholine Receptor–Mediated Protection of the Rat Heart Exposed to Ischemia Reperfusion

Spyros A Mavropoulos,[1,4] Nayaab S Khan,[1] Asaph CJ Levy,[4] Bradley T Faliks,[4] Cristina P Sison,[2,4] Valentin A Pavlov,[3,4] Youhua Zhang,[5] and Kaie Ojamaa[1,4,5]

[1]Center for Heart and Lung Research, [2] Biostatistics Unit, and [3] Center for Biomedical Sciences, The Feinstein Institute for Medical Research, Northwell Health, Manhasset, New York, United States of America, [4]Hofstra Northwell School of Medicine, Hofstra University, Hempstead, New York, United States of America, and [5]Department of Biomedical Sciences, New York Institute of Technology College of Osteopathic Medicine, Old Westbury, New York, United States of America

Reperfusion injury following acute myocardial infarction is associated with significant morbidity. Activation of neuronal or non-neuronal cholinergic pathways in the heart has been shown to reduce ischemic injury, and this effect has been attributed primarily to muscarinic acetylcholine receptors. In contrast, the role of nicotinic receptors, specifically α-7 subtype (α7nAChR), in the myocardium remains unknown, which offers an opportunity to potentially repurpose several agonists/modulators that are currently under development for neurologic indications. Treatment of *ex vivo* and *in vivo* rat models of cardiac ischemia/reperfusion (I/R) with a selective α7nAChR agonist (GTS21) showed significant increases in left ventricular developing pressure and rates of pressure development, without effects on heart rate. These positive functional effects were blocked by co-administration with methyllycaconitine (MLA), a selective antagonist of α7nAChRs. *In vivo*, delivery of GTS21 at the initiation of reperfusion reduced infarct size by 42% ($p < 0.01$) and decreased tissue reactive oxygen species (ROS) by 62% ($p < 0.01$). Flow cytometry of MitoTracker Red–stained mitochondria showed that mitochondrial membrane potential was normalized in mitochondria isolated from GTS21-treated compared with untreated I/R hearts. Intracellular adenosine triphosphate (ATP) concentration in cultured cardiomyocytes exposed to hypoxia/reoxygenation was reduced ($p < 0.001$), but significantly increased to normoxic levels with GTS21 treatment, which was abrogated by MLA pretreatment. Activation of stress-activated kinases JNK and p38MAPK was significantly reduced by GTS21 in I/R. We conclude that targeting myocardial α7nAChRs in I/R may provide therapeutic benefit by improving cardiac contractile function through a mechanism that preserves mitochondrial membrane potential, maintains intracellular ATP and reduces ROS generation, thus limiting infarct size.

Online address: http://www.molmed.org
doi: 10.2119/molmed.2017.00091

INTRODUCTION

Cardiac contractility, pacemaker activity and conduction are controlled by the autonomic nervous system, with catecholaminergic and cholinergic signals originating from sympathetic and parasympathetic neural pathways. An imbalance in neurotransmission from these two opposing neural pathways with increased adrenergic and diminished cholinergic activities has been observed in heart failure and systemic hypertension, and with increasing age (7,9,33). Experimental studies aimed at reducing cholinergic neural activity using mice deficient in muscarinic-acetylcholine receptors (AChR) or vesicular acetylcholine transporters (VAChT) have clearly shown that the parasympathetic nervous system has a protective role in maintaining cardiac function (24,25). Furthermore, vagus nerve stimulation in animal studies and in patients with heart failure has shown improvement in cardiac function, suggesting that cholinergic-pathway activation may provide therapeutic benefit (5,18,45,53,). Other studies using drugs to augment the parasympathetic nervous system or influence vagal tone, including acetylcholinesterase inhibitors such as donepezil or pyridostigmine, show evidence of improved ventricular remodeling and autonomic function in animal models of heart failure or after myocardial infarction (13, 26,32, 37,42). Studies of patients treated with these drugs for Alzheimer's dementia have reported reduced adverse cardiac events, including myocardial infarction and death (31).

Address correspondence to *Kaie Ojamaa, Department of Biomedical Sciences, New York Institute of Technology College of Osteopathic Medicine, Old Westbury, NY, 11568, USA. Phone: (516) 686-1016; Fax: (516) 686-3832; E-mail: kojamaa@nyit.edu*
Submitted May 26, 2017; Accepted for Publication May 31, 2017; Published Online (www.molmed.org) June 8, 2017.

Feinstein Institute for Medical Research
Northwell Health™

Reports documenting the synthesis and secretion of acetylcholine (ACh) by the cardiomyocyte further implicate the importance of non-neuronal cholinergic signaling mechanisms in maintaining the physiologic health of the myocardium (16,35,36). Evidence from various transgenic mouse models suggests that this autocrine/paracrine action of ACh is cardioprotective under stressful conditions, such as cardiac hypertrophy and failure, as well as ischemic injury (17,39). However, the molecular mechanisms by which ACh elicits these effects remain unclear. ACh initiates its cellular signal by activating G-protein–coupled muscarinic receptors (M2, M3) or by binding to nicotinic receptors (nAChR) that are ligand-gated ion channels, and both receptor types are present in the heart (2,10). Although the well-known effects of neuron-derived ACh on heart-rate response have been attributed to muscarinic receptor activation on atrial cells, the effects of ACh acting on nicotinic receptors remain largely unknown (reviewed in [40]). Dvorakova *et al.* (10) showed by immunohistochemistry of rat hearts that nicotinic α7 subunits localize to cardiac neurons, fibroblasts and cardiomyocytes, and that α2/α4 subunits concentrate at myocyte intercalated discs. More recently, Gergalova *et al.* (11,12) identified α7nAChRs in liver mitochondria outer membranes that function to regulate mitochondrial permeability transition pore (mPTP) formation through kinase-mediated signaling pathways, thus preventing cytochrome *c* release and attenuating apoptosis. The presence of α7nAChRs in cardiac mitochondria has not been reported. However, this finding would be of particular significance in cardiac ischemia/reperfusion (I/R), since reactive oxygen species (ROS) generation and influx of calcium, which occur during reperfusion, trigger formation of the mPTP, leading to depolarization of the mitochondrial membrane, organelle swelling and rupture, release of cytochrome c and cell death (14).

We focused the present study on the potential therapeutic utility of activating nicotinic receptors, specifically α7nACh, to reduce reperfusion injury after acute myocardial infarction. The rationale for the study was that the process of reperfusion after a period of ischemia can further induce cardiomyocyte death, for which no effective treatment currently exists, and intervention at this time period may be most effective in decreasing myocyte injury and subsequently enhancing recovery of cardiac function (reviewed in [14]).

MATERIALS AND METHODS

Reagents

GTS-21 (3-(2,4-dimethoxy-benzylidene) anabaseine dihydrochloride; DMXB-A) and methyllycaconitine citrate salt hydrate (MLA) were purchased from Sigma Aldrich (St. Louis, MO) and galantamine hydrobromide from Calbiochem (San Diego, CA). Cell culture reagents and media were purchased from Gibco (ThermoFisher Scientific, Waltham, MA). All other reagents and chemicals were of the highest quality and purity, purchased from commercial sources.

Animal Models

All animals were treated in accordance with the National Institutes of Health *Guidelines for the Use and Care of Laboratory Animals* (HHS Pub. No. 85-23), and study protocols were approved by the Institutional Animal Care and Use Committee of The Feinstein Institute for Medical Research.

Isolated perfused hearts. Animals were randomized to treatment groups on the day of study. Hearts from male Sprague-Dawley rats (310g ± 20g) (Taconic Biosciences, Inc., Hudson, NY) were isolated and perfused in retrograde mode at a constant pressure of 90 mmHg at 37°C as previously described (19). Briefly, rats were heparinized (100 Units) prior to anesthesia (sodium pentobarbital, 60 mg/kg intraperitoneally), hearts rapidly removed and perfused with modified Krebs-Henseleit buffer (KHB; Sigma Aldrich), which was freshly prepared with the addition of calcium chloride and sodium bicarbonate according to the manufacturer's instructions. Contractile function was assessed using a pressure transducer coupled to a water-filled latex balloon inserted into the left ventricle through the mitral valve and inflated to an initial end diastolic pressure (EDP) of ~5 mmHg. Hearts were equilibrated for 10 min with KHB and then perfused with KHB containing vehicle or drugs for 10 min prior to initiation of normothermic global ischemia, by stopping perfusion for 30 min, followed by 40 min reperfusion with KHB. Drugs were delivered prior to the ischemic period, because the perfusion flow rate is very low following ischemia, preventing the rapid delivery of drugs. Left ventricular (LV) pressures were recorded continuously throughout the perfusion period, and functional values for each heart were calculated as percent of values recorded at the end of the 10 min equilibration period. Function measurements recorded were: left ventricular developed pressure (LVDP), rate of pressure development and rate of relaxation (± dP/dt) and heart rate (HR). Work product (WP) was calculated by multiplying LVDP by HR. Drug concentrations delivered were: GTS21 (1.6×10^{-8} M), methyllycaconitine (MLA) (2.33×10^{-7} M), galantamine (5×10^{-8} M) and combined GTS21 + MLA (same dosing). Hearts were excluded from the study if, during the equilibration period, perfusion rate was <10 mL/min, HR was <100 bpm, LVDP was <100 mmHg or sustained arrhythmic events were recorded. Perfusion control hearts were not subject to ischemia but were perfused for the same length of time as I/R hearts.

***In vivo* studies.** Female Sprague-Dawley rats (230–300 g) (Taconic Biosciences, Inc.) were randomized to sham surgery or I/R, treated with either saline or GTS-21. The animals were fully anesthetized with sodium pentobarbital (80 mg/kg), the chest and neck were shaved and the skin cleaned with betadine and alcohol. Animals were orally intubated and mechanically ventilated (Harvard Apparatus, Holliston, MA) with room air at a tidal volume of 1 mL/100 g body weight and a respiratory rate of 60 breaths/min.

Core body temperature was maintained at ~36°C using a heating pad and was monitored continuously. A left thoracotomy exposed the heart, the pericardial sac was opened and the left anterior descending (LAD) coronary artery at the level of the left atrium was ligated with 6-0 braided silk suture around a 4 mm length of PE-50 tubing to prevent vessel injury. The LAD was occluded for 30 min, and then reperfusion was initiated by removing the PE tubing. At the start of reperfusion, GTS-21 (0.125 mg/kg in 0.2 mL saline) or saline was injected as a bolus via a cannula (PE-50 tubing) placed in the right femoral vein or the left common carotid artery. After 60 min of reperfusion, the LAD was occluded again by tightening the suture, and 2 mL of Evans blue dye solution (7%) was injected into the circulation via the left common carotid artery to delineate the perfused heart tissue from the nonperfused area at risk (AAR). After approximately 2 min of perfusion with dye, the heart was excised and sectioned along the short axis into five or six 2 mm slices that were incubated in 2,3,5-triphenyltetrazolium chloride solution (TTC, 1% in phosphate-buffered saline [PBS]; Sigma Aldrich) for 30 min at 37°C to define viable and nonviable tissue within the AAR. Infarct size and AAR were measured by one individual as previously described (23).

In Vivo Hemodynamic Analysis

Left ventricular hemodynamic measurements were recorded in animals that were not used to measure infarct size. At the end of the I/R period described above, a 1.4-Fr Millar pressure catheter (SPR-671; Millar Instruments, Houston, TX) was inserted into the right carotid artery and advanced into the left ventricle. LV pressures were recorded over a 5 min period and data were collected using PowerLab 8/30 acquisition system (AD Instruments, Colorado Springs, CO) and analyzed with LabChart Pro software. Control LV pressures were obtained from a separate group of sham operated animals that underwent identical experimental surgical procedures without occlusion of the LAD.

Tissue Homogenization, Fractionation and Immunoblot Analysis

Hearts were excised, rapidly frozen in liquid nitrogen and stored at –80°C. For immunoblot analysis, the LV free wall from the *in vivo* studies was used, whereas the entire LV from perfused hearts was used. Frozen tissue was homogenized in 10 volumes of ice-cold buffer (50 mM Tris HCl, pH 7.5, 150 mM NaCl, 2 mM EDTA, phosphatase/protease inhibitor cocktail; Cell Signaling Technologies, Danvers, MA) using glass mortar and motor-driven Teflon pestle. The homogenate was centrifuged at 1,000*g* for 10 min at 4°C, and the resulting supernatant was collected and centrifuged at 10,000*g* for 30 min at 4°C to obtain the cytosolic fraction. Protein concentrations were measured using Micro BCA Assay (Pierce, Rockford, IL). Samples of 50 μg proteins were resolved on 10% sodium dodecyl sulfate polyacrylamide gel electrophoresis and transferred onto nitrocellulose membranes, which were treated as necessary with Miser Antibody Extender Solution NC (Thermo Scientific, Rockford, IL). Equal amounts of each sample were run on parallel gels to quantify total and phosphorylation of the stress-activated proteins. Immunoblots were probed overnight at 4°C using the following primary antibodies (dilutions): phospho-JNK (1:10,000) (cat. no. 9251), JNK (1:10,000) (cat. no. 9252S), phospho-p38 MAPK (1:10,000) (cat. no. 9211) and p38 MAPK 1:10,000 (cat. no. 9212) from Cell Signaling Technologies; α7 nicotinic acetylcholine receptor (1:500) (cat. no. ANC-007; Alomone Labs, Jerusalem, Israel); and GAPDH (1:100,000) (Sigma Aldrich). Signals from horseradish peroxidase–conjugated secondary antibodies were developed using chemiluminescence reagent (Thermo Scientific) and detected on either x-ray film or ChemiDoc MP (BioRad, Hercules, CA). Images on film were quantified using ImageJ (National Institutes of Health, Bethesda, MD), and ChemiDoc images were quantified using BioRad Image Lab.

Measurement of Tissue ROS

At the end of the I/R protocol for the *in vivo* studies, hearts were removed, rinsed in ice-cold saline and embedded in tissue-freezing medium for cryosectioning. Eight micrometer thick cross-sectional slices were cut serially, starting from the basal area of the heart, and mounted on histological slides, then incubated in PBS for 30 min. The slides were stained with dihydroethidium (DHE) for 30 min as previously published (22). Images of the stained slides were obtained immediately using a Leica DMI 4000B microscope (Leica Microsystems Inc., Buffalo Grove, IL) at 200 × magnification with an excitation wavelength of 551 nm. Light intensity measurements were recorded from three independent areas of each tissue slice, and data from three slices per heart were analyzed. Fluorescence intensity was quantified using Image Studio Lite v.3.1 (Licor, Lincoln, NE) and presented as arbitrary units.

Isolation of Mitochondria

Mitochondria were isolated from perfused LV tissue (60 mg) immediately at the end of the protocol, using a commercially available mitochondrial isolation kit (Sigma Aldrich) according to the manufacturer's instructions. This model of normothermic global ischemia assumes that the entire LV is involved. In brief, tissue was minced on a glass plate cooled on ice, washed in ice-cold buffer (10 mM HEPES, pH 7.5, 200 mM mannitol, 70 mM sucrose, 1 mM EGTA), and then digested with trypsin for 20 min at 37°C. Digestion was stopped with bovine serum albumin, and the tissue was homogenized using a Teflon-on-glass homogenizer. The homogenate was centrifuged at 600*g* for 5 min at 4°C, and the supernatant collected and centrifuged at 11,000*g* for 10 min at 4°C to obtain the pellet containing the mitochondria. The pellet was resuspended in storage buffer (10 mM HEPES, pH 7.5, 0.25 M sucrose, 1 mM ATP, 0.08 mM ADP, 5 mM sodium succinate, 2 mM K_2HPO_4, 1 mM DTT), and aliquots for single use were stored at –80°C.

Measurement of Mitochondrial Membrane Potential

Isolated heart mitochondria (25 μg protein in 5 μL) from the various treatment groups were added to 950 μL assay buffer (20 mM MOPS pH 7.5, 110 mM KCl, 10 mM ATP, 10 mM $MgCl_2$, 10 mM sodium succinate, 1 mM EGTA) plus 45 μL of storage buffer provided in the mitochondrial isolation kit described above. MitoTracker Red FM (Molecular Probes, Eugene, OR) was added to the mitochondria to achieve a final concentration of 2×10^{-7} M and incubated on ice for 30 min. Mitochondrial fluorescence was analyzed with an LSR Fortessa flow cytometer (Becton Dickinson, Franklin Lakes, NJ). Excitation was achieved using the 640 nm laser. Gating parameters on the flow cytometer were established using a control mitochondrial sample and adjusting the voltages for the forward scatter, side scatter and MitoTracker Red laser so that the histograms for each laser had population peaks $>10^2$ but $<10^3$. All samples were run one after the other on the same day with the same settings. Samples of mitochondria isolated from perfusion control hearts were used to establish the gating parameters, and 10,000 events were collected for each sample. GTS21-treated I/R and vehicle-treated I/R mitochondria samples were analyzed using the established control gating parameters, and the data are expressed as the percent of total mitochondria in each treatment sample that localized within the established control mitochondria gating parameters. The FACS data were analyzed using FlowJo software v10 (Ashland, OR). Mitochondria isolated from untreated hearts were incubated with either antimycin A (2×10^{-4} M) or oligomycin (10^{-6} M) (ThermoFisher Scientific, Ward Hill, MA) for 30 min prior to MitoTracker Red staining and analyzed by fluorescence-activated cell sorting (FACS) to identify the gating parameters of mitochondria that were maximally depolarized or hyperpolarized, respectively.

Neonatal Rat Ventricular Myocytes (NRVMs)

Hearts of 2-d-old rat pups (Sprague-Dawley) were digested with collagenase to isolate ventricular myocytes as previously published (21). Experiments were repeated on a second independent isolation of primary ventricular myocytes to verify the results obtained. In brief, NRVMs were plated on collagen-coated 35 mm dishes and cultured for 48 h in Dulbecco's Modified Eagle's Medium (DMEM)/F12 medium containing 10% fetal bovine serum, L-glutamine and cytosine β-D-arabino-furanoside (Ara C) (10^{-5} M) that was refreshed daily. Cells were exposed to normoxic or hypoxic conditions for 8 h, followed by treatment with vehicle or GTS21 (10^{-9} M) during reoxygenation. The 8-h-hypoxic time period initiated apoptotic signaling events (data not shown). Cells were harvested at various time points after initiation of reoxygenation. In normoxic conditions, cells were maintained in low-glucose DMEM containing insulin (120 IU/L), transferrin (5 mg/L) and selenium (5 μg/L) (ITS), while cells in hypoxic conditions were maintained in DMEM without insulin, glucose and pyruvate. During reoxygenation, media were replaced with low-glucose DMEM containing TS without insulin. Hypoxic conditions were established by placing the cell culture plates in a small airtight plexiglass chamber (BioSpherix, Parish, NY) infused with a mixture of 95% nitrogen/5% CO_2 gas to maintain <0.2% oxygen content under humidified 37°C conditions. For normoxia and reoxygenation conditions, cells were placed in a standard humidified cell culture incubator maintained at 37°C and room air/5% CO_2.

For immunocytochemistry, the cardiomyocytes were plated onto collagen-coated glass coverslips placed in 6-well plates and cultured for 4 d as described above. After cells were washed with Hank's Balanced Salt Solution, they were fixed with freshly prepared 2% paraformaldehyde in PBS for 15 min, followed by several washes in PBS with 1% glycine. Cells were permeabilized with 0.1% TritonX-100 in PBS, then washed and blocked with 10% goat serum for 1 h at room temperature. Cells were incubated overnight at 4°C with the following primary antibodies diluted in 1% goat serum/PBS solution: α7 nicotinic acetylcholine receptor diluted 1:50 (cat. no. ANC-007; Alomone Labs), isotype-control rabbit IgG diluted 1:25 (cat. no. sc-2027; Santa Cruz Biotechnology, Dallas, TX). After several washes, cells were incubated with secondary antibody Alexa Fluor 488 goat anti-rabbit IgG diluted 1:100 (cat. no. A-11008; Invitrogen, Waltham, MA) and for F-actin staining, TRITC-conjugated phalloidin diluted 1:500 (Sigma Aldrich,) for 1 h at room temperature and protected from light. The coverslips were mounted onto slides using Fluoroshield Mounting Medium containing 4',6-diamidino-s-phenylindole (Abcam, Cambridge, MA) for nuclear staining. Images were captured at 630 × magnification using the Zeiss Axiocam ER C5S (Carl Zeiss AG, Oberkochen, Germany). Wavelength settings and exposure times were maintained when comparing fluorescence emitted from cells incubated with control IgG isotype and with anti-α7nAChR antibody.

Western Blot Analysis of NRVM

Cells were homogenized in lysis buffer containing final concentrations of 50 mM Tris HCl, pH 7.4, 150 mM NaCl, 1 mM EDTA, 1% NP-40 and protease/phosphatase inhibitor (Cell Signaling Technologies, cat. no. 5872), followed by centrifugation at 13,000 rpm for 10 min at 4°C. Protein concentrations of the supernatants were measured using Micro BCA Assay, and samples of 30 μg protein were resolved on 10% sodium dodecyl sulfate polyacrylamide gel electrophoresis and transferred onto nitrocellulose membranes as described above. Phospho-proteins and their total nonphosphorylated isoforms were analyzed consecutively by stripping the anti-phosphoprotein antibody, then incubating with the anti-nonphosphoprotein antibody on the same blot. Primary antibodies used for immunoblot analysis

were from Cell Signaling Technologies: phospho-p44/42 MAPK (cat. no. 9106, 1:3000), p44/42 MAPK (cat. no. 9102, 1:10,000), pJNK, JNK, p-p38^{MAPK} and p38^{MAPK}. Secondary antibodies used were either goat anti-rabbit (BioRad, cat. no. 170-6515) or goat anti-mouse (BioRad, cat. no. 170-6516) IgG conjugated with horseradish peroxidase. Proteins were detected using chemiluminescence reagent Super Signal West Femto (ThermoFisher Scientific, cat. no. 34096), visualized using Chemidoc-MP (BioRad), and densitometric analysis was performed using Image Labs software (BioRad).

Adult Human Cardiomyocytes (AC16)

AC16 cells (adult human cardiac muscle cell line; ATCC, Bethesda, MD) were cultured as previously published (28). These immortalized cells, as originally developed and described by Davidson *et al.* (4), exhibit many biological and morphological characteristics of cardiac muscle cells. This cell line is not listed by the International Cell Line Authentication Committee as misidentified.

FACS Analysis of α7nAChR Expression on AC16 Cells

Adherent cultured AC16 cells were dissociated with an enzyme-free buffer (Gibco/ThermoFisher, Grand Island, NY) and collected by centrifugation. Cells were resuspended in MACS buffer (Miltenyi Biotec, Gladbach, Germany) to a final density of 300,000 cells/tube, and then incubated for 30 min on ice with anti-α7nAChR antibody (0.5 μg/tube) (cat. no. ANC-007; Alomone) or antibody preincubated for 1 h with its blocking immunogen or isotype control IgG. Cells were then washed twice with MACS buffer and incubated with PE-conjugated anti-rabbit antibody (2μg/mL) (cat. no. 4052-09; Southern Biotech, Birmingham, AL) for 30 min on ice, then washed twice and resuspended in MACS buffer. Identification of cell-associated α7nAChR was determined by flow cytometry (LSR Fortessa). Excitation was achieved using a 488 nm laser with a 575/26 filter. Gating parameters were FCS at 110 V with a threshold of 5000, SCC at 308 V and PE at 214 V; 30,000 events were collected for each sample. The FACS data were analyzed using FlowJo software v10.

Measurement of Intracellular ATP Concentration

AC16 cells were grown on collagen-coated 6-well dishes at a density of 200,000 cells/well in DMEM containing 10% fetal bovine serum. Cells were exposed to normoxic or hypoxic conditions (described above) for 6 h, followed by 1 h reoxygenation in low-glucose serum-free DMEM with or without GTS21 (10^{-9} or 10^{-8} M) or pretreated with MLA (10^{-7} M). The 6-h-hypoxic period was chosen based on our prior studies showing induction of apoptotic events (data not shown). Cells were harvested in 200 μL 50 mM Tris-1mM EDTA pH 7.4 buffer containing 0.2% NP40, flash-frozen and stored at –80°C. Samples were lysed by passing through a 26 G needle, an aliquot used for protein determination (Micro BCA Assay, Pierce) and 25 μL boiled in 975 μL Tris-EDTA for 2 min. The boiled sample was clarified at 1,000*g* at 4°C and the final supernatant diluted 1:4000 with water. A luciferase/luciferin reaction mixture was prepared by adding luciferase (1.2×10^9 U/mL; Sigma Aldrich) and luciferin (0.2 mM; Sigma Aldrich) to buffer containing 50 mM Tris-acetate, pH 7.9, 10 mM magnesium acetate, 1 mM EGTA and 100 mM DTT. Ten μL of diluted sample was added to 100 μL of the luciferase/luciferin reaction mixture and read immediately in a luminometer (Turner Model TD-20, Madison, WI). ATP content was calculated using a standard curve, and values were normalized to protein concentration in the sample.

Statistical Analysis

Data are presented as the mean ± standard error (or standard deviation, as indicated). Sample numbers per group are indicated in the Results section and figure legends. Statistical analysis was performed using two-tailed Student *t* test or one-way analysis of variance (ANOVA), followed by post hoc analysis using Newman-Keuls test. All data passed tests for normality distribution and equal variance (SigmaStat 3.1; Systat Software, Richmond, CA). For statistical analysis of the five outcome variables measured in the perfused hearts (LVDP, + dP/dt, -dP/dt, HR, WP) that were recorded continuously during the reperfusion period, a mixed model applied to repeated-measures ANOVA (RMANOVA) was performed on values at 0, 5, 10, 15, 20 and 30 min to determine if measurements varied significantly over time and between the four treatment groups (I/R + vehicle, I/R + GTS21, I/R + GTS + MLA, I/R + MLA). Adjusted pairwise comparisons were made between treatment groups at each time point, and differences in values were considered statistically significant at $p < 0.01$. In the galantamine studies, RMANOVA was used for comparisons of vehicle- and galantamine-treated perfused I/R hearts with respect to the patterns of change in each of the five outcome variables, except that log-transformed values of the raw data were used, since the standard model assumptions were not met for all outcome variables. Results were then back-transformed and are reported using the geometric means and corresponding standard errors. Statistical analysis was performed using SAS v9.3 (Cary, NC).

RESULTS

Cholinergic Pathway Activation Improves LV Function during Reperfusion

Isolated perfused heart experiments. The experimental protocol for perfusion of the isolated rat heart is depicted in Figure 1A. As evident in Figure 1B, at 90 min total perfusion time, the LVDP of control hearts decreased below 80% of their pre-ischemia values. Therefore, assuming that contractile function of all isolated perfused hearts deteriorates

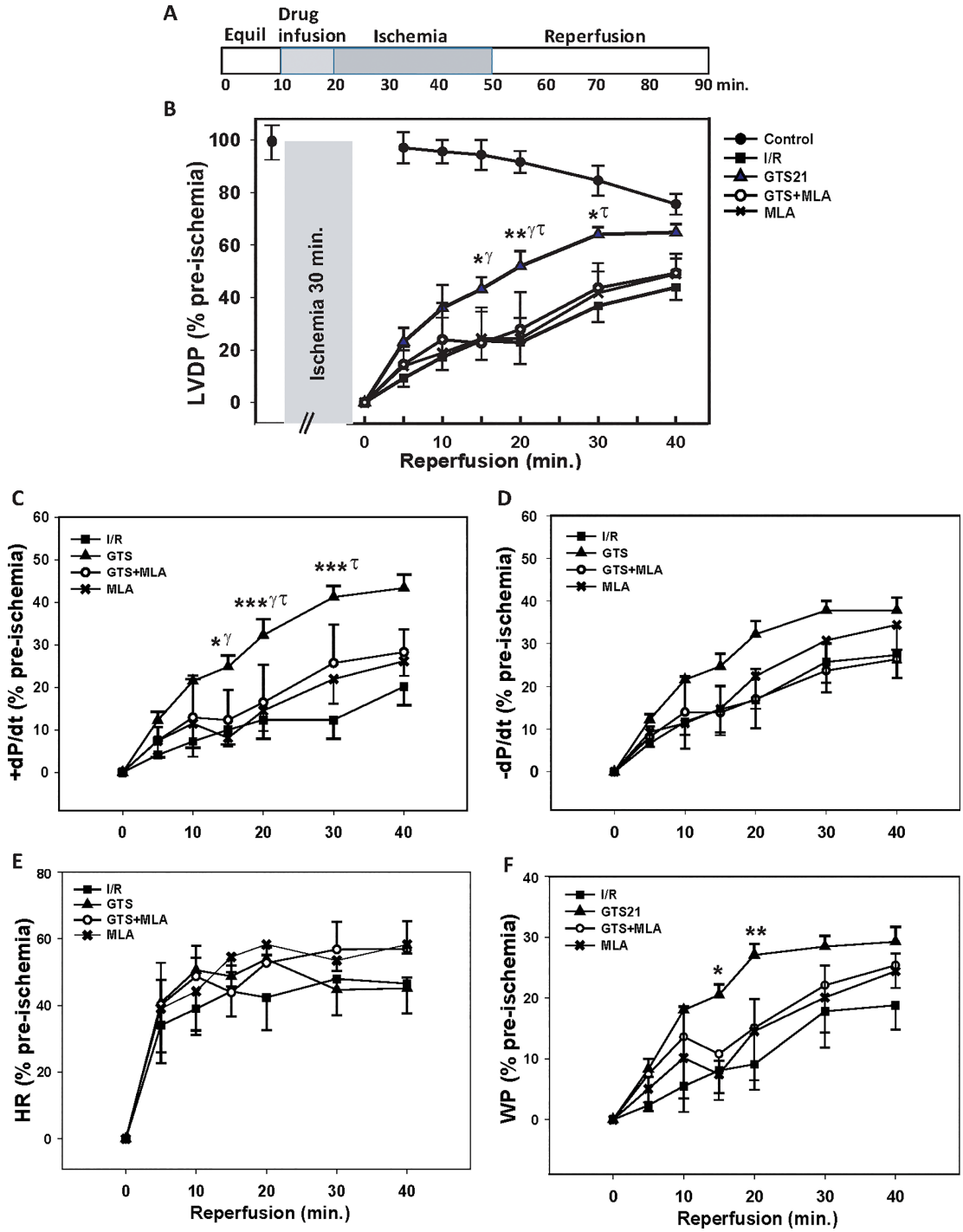

Figure 1. α7nAChR activation with GTS21 treatment improved contractile function of I/R perfused rat hearts. (A) Experimental protocol of the rat heart perfusion studies. Equil, equilibration period. (B–F) LV pressures were recorded during the 40 min reperfusion period and five outcome variables (LVDP, + dP/dt, -dP/dt, heart rate (HR), work product (WP)) were measured at 0, 5, 10, 15, 20, 30 and 40 min and are expressed as percent of the value measured at the end of the equilibration period (% pre-ischemia). Data points represent treatment group mean ± SE. Perfusion control (●, n = 5); I/R + vehicle (■, n = 4); I/R + GTS21 (▲, n = 6); I/R GTS21 + MLA (○, n = 3). I/R + MLA (**x** , n = 3). RMANOVA performed on the five outcome variables measured at six time points (0–30 min) showed significant group × time interactions in (B), (C) and (F), and pairwise comparisons between the four treatment groups showed significance at individual time points as indicated: $^{*}p < 0.01$ versus I/R, $^{**}p < 0.001$ versus I/R, $^{***}p \leq 0.0001$ versus I/R, $^{\tau}p < 0.01$ versus GTS + MLA, $^{\gamma}p < 0.01$ versus MLA.

with perfusion time, the statistical analysis that was used for these studies utilized LV pressures recorded from 0 to 30 min reperfusion.

In preliminary studies, the optimum treatment dose of GTS21 was determined empirically by measuring LV function through a concentration range from 10^{-7} to 10^{-9} M and was the dose that produced the highest recovery of LVDP during reperfusion (data not shown). Thus, delivery of GTS21 at the optimum dose (1.6×10^{-8} M) to perfused rat hearts prior to ischemia significantly improved LV function during the reperfusion period compared with vehicle-treated ischemic hearts, and this effect of GTS21 was blocked by co-administration of MLA, a selective α7nAChR antagonist. This effect reached statistical significance at 20 and 30 min of reperfusion (Figure 1B). MLA treatment alone of the I/R hearts had no effect on any outcome variables, thus supporting the specificity of its effect. In addition to LVDP, the maximum rate of LV pressure development (+ dP/dt) showed significant improvement with GTS21 treatment versus vehicle-treated I/R (Figure 1C), whereas the improvement in –dP/dt did not reach statistical significance (Figure 1D). These positive effects of GTS21 treatment on LV function occurred without any significant changes in heart rate (Figure 1E). The increase in WP, a function of heart rate × LVDP, with GTS treatment reached significance at 15 and 20 min of reperfusion (Figure 1F). GTS21 treatment of control perfused hearts that were not exposed to ischemia had no significant effect on LV pressure measurements recorded over 30 min (data not shown). End diastolic pressure (EDP) increased during the final 10–15 min of the ischemic period to 37 ± 3 mmHg in I/R hearts, which decreased to 21 ± 6 mmHg with GTS. The maximum increases in EDP for the MLA and MLA + GTS treated groups were 44 ± 15 and 36 ± 11 mmHg, respectively. However, EDP data were not statistically different among the groups. Irregular rhythmic events occurred early in the reperfusion period for all hearts regardless of treatment. The total time spent in arrhythmia recorded as seconds during 30 min of reperfusion were 325 ± 208, 353 ± 144, 469 ± 239 and 662 ± 296 for the I/R + vehicle, I/R + GTS, I/R + MLA and I/R + GTS + MLA groups, respectively. Differences among groups were not statistically significant.

Galantamine (5×10^{-8} M), a cholinesterase inhibitor and positive allosteric modulator of α7nAChR, was similarly delivered prior to ischemia and resulted in significantly higher LV functional measurements without HR changes compared with vehicle-treated I/R hearts (Table 1).

***In vivo* cardiac I/R.** Studies were undertaken to evaluate the effects of GTS21 treatment on rat myocardial I/R injury *in vivo*. GTS21 was delivered intravenously at the initiation of reperfusion in the dose range of 0.06–1.0 mg/kg, and it was determined that 0.125 mg/kg produced the maximum recovery of LV function after 60 min of reperfusion. This dose of GTS21 was used in all experiments. All measurements of LV function, including LVDP, + dP/dt and -dP/dt, recorded at 60 min of reperfusion showed significant improvement with GTS21 treatment compared with vehicle-treated animals (Table 2). Similar to the perfused heart experiments, heart rate was unaffected by GTS21. Work product was significantly higher ($p < 0.001$) in GTS-treated than vehicle-treated I/R animals, but remained lower ($p < 0.05$) than in sham-operated animals.

The improvement in LV function observed in response to GTS21 treatment of I/R animals was further supported by the significant ($p < 0.01$) reduction of myocardial infarct size relative to AAR (INF/AAR, %) compared with vehicle-treated I/R hearts (32 ± 4% versus 55 ± 3%, respectively) (Figure 2A). This reduction in myocardial tissue injury was

Table 1. Left ventricular pressure measurements of isolated rat hearts recorded after ischemia during the reperfusion period.

†Function, %pre-ischemia	I/R + vehicle	I/R + Galantamine
LVDP	36.8 ± 12.4	72.6 ± 17.6*
+dP/dt	20.2 ± 8.7	46.9 ± 14.7*
–dP/dt	25.7 ± 14.2	45.6 ± 11.3*
HR	48.0 ± 21.7	53.4 ± 7.8
WP	17.8 ± 11.9	38.5 ± 10.5*

†Functions are LV pressures calculated as percent pre-ischemia values. Values are mean ± SD recorded at 30 min of reperfusion. LVDP, LV developed pressure; ± dP/dt, min or max developed pressure over time; HR, heart rate; WP, work product. RMANOVA was performed on data recorded between 0 and 30 min of reperfusion. Adjusted pairwise comparisons between the treatment groups show significant differences, with *$p < 0.05$ versus vehicle; n = 4/group.

Table 2. Myocardial contractile function measured *in vivo* in a rat model of I/R.

Function (post-I/R)	Sham surgery (n=6)	I/R + veh (n=10)	I/R + GTS (n=10)
LVDP (mmHg)	119 ± 18	66 ± 15***	97 ± 14*†
+dP/dt (mmHg·sec^{-1})	5542 ± 1106	3640 ± 1441**	5648 ± 576†
-dP/dt (mmHg·sec^{-1})	-6860 ± 1580	-3061 ± 1487***	-5636 ± 1423†
HR (bpm)	396 ± 27	380 ± 40	395 ± 40
WP (mmHg·bpm)	47175 ± 9000	25544 ± 7953***	38393 ± 6630*†

One-way ANOVA with Student-Neuman-Keuls post hoc pairwise multiple-comparison test performed. *$p < 0.05$, **$p < 0.01$, ***$p < 0.001$ versus sham; †$p < 0.001$ versus I/R + veh; values are mean ± SD; (n) = number of animals/group.

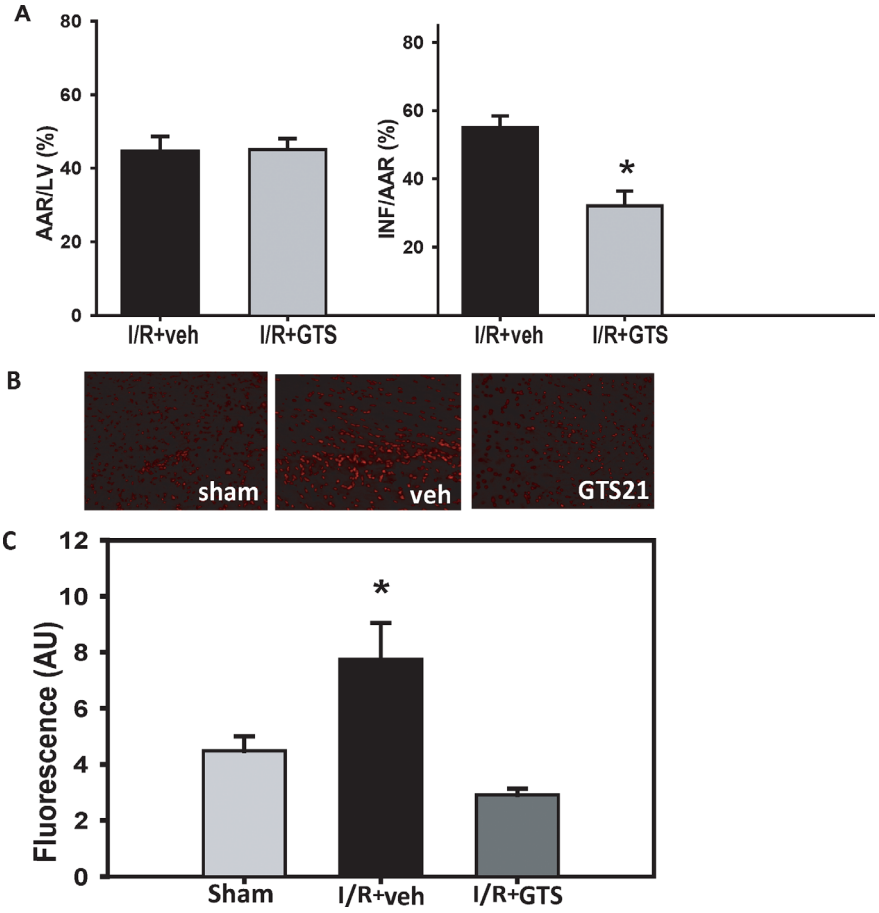

Figure 2. GTS21 treatment at reperfusion reduced infarct size and ROS and improved contractile function *in vivo* in a rat model of I/R. (A) Myocardial area at risk (AAR) as percent of LV area in rats receiving vehicle (veh, n = 6) or GTS21 (GTS, n = 6) (no statistical difference between groups); data are mean ± SE. Infarct size (INF) expressed as percent AAR. Statistical significance was determined by Student *t* test. *$p < 0.01$ versus I/R + veh. (B) Representative images of DHE staining of 8 μm frozen sections of LV free wall in sham, I/R + veh and I/R + GTS21 groups; 200 × magnification; excitation wavelength, 551 nm. (C) Quantitation of DHE fluorescence (AU, arbitrary units) in microscopic images using Image Studio Lite v3.1. Staining intensity was measured in three independent areas in three sequential sections per heart. n = 5 hearts/group; bar graph represents group mean ± SE. Statistical significance determined by one-way ANOVA. *$p < 0.01$ versus sham and I/R + GTS.

reflected in a significant ($p < 0.01$) reduction in ROS generation as measured by fluorescence microscopy of dihydroethidium (DHE) staining of cross-sectional LV slices (Figure 2B). Quantitation of the intensity of DHE staining showed that the increase of ROS in I/R hearts was significantly reduced in the GTS21-treated animals to a level that was not different from sham-operated control animals (Figure 2C).

Mitochondrial Membrane Potential Normalized by GTS21 Treatment

Mitochondria play an integral role in ROS generation and are key determinants of cell survival following I/R injury. To determine whether maintaining mitochondrial integrity was integral to the cytoprotective effects of GTS21 in myocardial I/R injury, mitochondria were isolated from perfused hearts to measure mitochondrial membrane potential (ΔΨM) using a mitochondrion-selective fluorophore (MitoTracker Red). FACS analysis was used to determine ΔΨM by measuring the fluorophore signal intensity in each mitochondrion (Figure 3A). To identify mitochondria membrane potentials as either hypopolarized or hyperpolarized, mitochondria samples were treated with antimycin A or oligomycin, respectively, and this is shown in the histogram as peak-a and peak-e (Figure 3B). Staining intensity of mitochondria isolated from I/R-vehicle treated hearts shows that these organelles were hyperpolarized (peak-d) compared with mitochondria from perfusion control (PC) (i.e., nonischemic) hearts (peak-b). GTS21 treatment of I/R hearts normalized mitochondrial membrane potentials (peak-c) to the ΔΨM measured in mitochondria from perfusion control hearts (peak-b). These results were quantified as the percent of total mitochondria in each treatment group that fell within the gating parameters encompassing mitochondria from perfusion control hearts, as indicated by the quadrangle in Figure 3A. As shown in the bar graph (Figure 3C), GTS21 treatment during I/R significantly increased ($p < 0.01$) the percent of mitochondria that localized within the established gating parameters, indicating that these mitochondria had the same ΔΨM as mitochondria from PC hearts.

GTS21 Attenuates I/R-Activated Intracellular Stress Pathways *In Vivo* and *Ex Vivo*

Expression of α7nAChR protein was not different in *ex vivo* perfused hearts or *in vivo* hearts subjected to I/R with or without GTS21 treatment (Figures 4A, B). To identify potential molecular mechanisms by which α7nAChR activation resulted in attenuated infarct size, mitochondrial preservation and improved contractile function, we measured intracellular signaling pathways known to regulate cell death and survival. Immunoblot analysis of stress-activated JNK and p38MAPK proteins in perfused hearts subjected to I/R showed significant increases in phosphorylation, thus

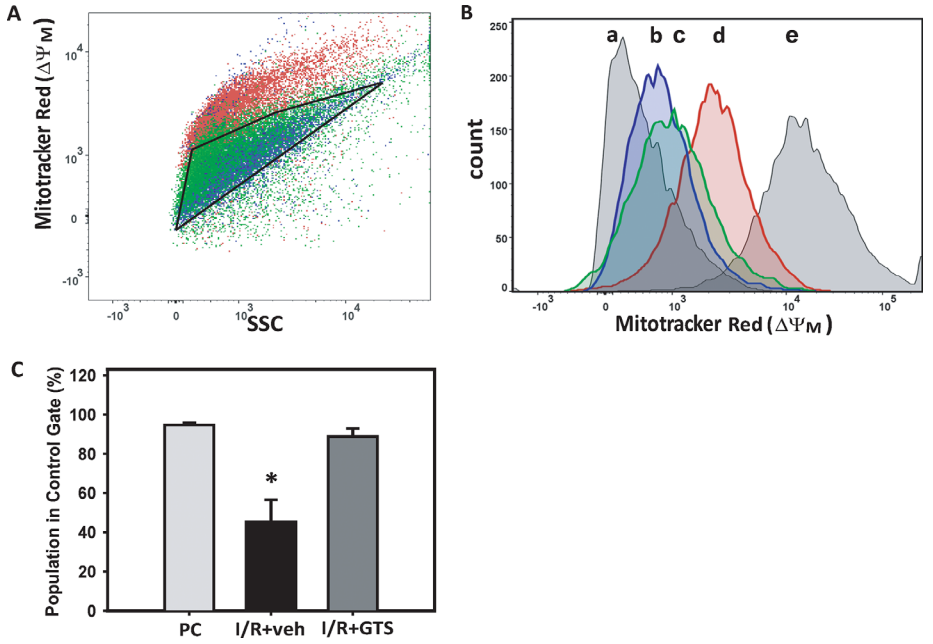

Figure 3. Membrane potential of mitochondria isolated from perfused rat hearts. (A) MitoTracker red dye used to measure mitochondria membrane potential (ΔΨm) by flow cytometry. Scatter plot showing individual mitochondria sorted by side scatter (SSC) and fluorescence intensity of MitoTracker dye. Red dots are mitochondria from I/R hearts, blue dots are from perfusion control (PC) nonischemic hearts and green dots are from GTS21-treated I/R hearts. The established gating parameter is indicated by the black lines encircling the PC mitochondria. (B) Histograms represent numbers of mitochondria counted and the intensity of MitoTracker red staining of those mitochondria isolated from each treatment group: a, antimycin A–treated mitochondria (hypopolarization); b, perfusion control (PC); c, I/R + GTS21; d, I/R + veh; e, oligomycin A–treated mitochondria (hyperpolarization). (C) Bar graph quantifying the percentage of total mitochondria in each treatment group that fell within the gating parameters established for the perfusion control mitochondria. Values are mean ± SE; PC, n = 3; I/R + GTS, n = 6; I/R + veh, n = 6 hearts. *$p < 0.01$ versus all groups; significance determined by one-way ANOVA.

activation, compared with PC hearts (Figure 4C). Notably, GTS21 treatment of I/R hearts attenuated this response to that observed in nonischemic perfused hearts (Figures 4C, D). Phosphorylation of AKT (protein kinase B) (Figure 4C) as well as ERK1/2, STAT3 and AMPK was not affected by the treatment conditions studied (data not shown).

α7nAChRs Are Expressed in Cultured Cardiomyocytes

We used primary cultures of NRVMs and an immortalized adult human ventricular myocyte line (AC16) to further investigate the molecular mechanisms by which α7nAChR activation may provide cytoprotection in the ischemic heart. Immunoblot analysis showed that α7nAChR protein was expressed in NRVM and AC16 lysates (Figure 5A). To further confirm that α7nAChRs are expressed on AC16 cells, which had not been previously reported, freshly dissociated cells were incubated with primary antibody directed at the extracellular amino-terminus of α7nAChR, then labeled with fluorescent-conjugated secondary antibody and analyzed by FACS (Figure 5B). The contour map (left panel) shows the distribution of cells, sorted by intensity of fluorescence (x-axis) of the anti-α7nAChR antibody versus forward scatter (y-axis). These data are quantified in the histogram (right panel) as cell count to antibody fluorescence intensity. The α7nAChR antibody binding to AC16 cells is represented by the higher fluorescence intensity peak-b, and this binding was largely prevented by preadsorption with the peptide immunogen, as indicated by the shift of peak-b to the lower-intensity peak-a. Peak-c represents cells incubated with isotype control IgG. These data confirm the presence of α7nAChR on AC16 cell membranes.

Fluorescence microscopy was used for immunolocalization of α7nAChRs in NRVMs. In Figure 5C, cells that stained for F-actin also showed strong fluorescence staining for α7nAChRs (a7nR), whereas F-actin–positive cells incubated with isotype control IgG showed no cell-specific fluorescence. Exposure times and wavelength settings were identical for these cells, grown on two separate coverslips. Micrographs in Figure 5D show NRVMs plated on separate coverslips incubated with either anti-α7nAChR antibody or the isotype control IgG, showing strong α7nAChR (a7nR) immunofluorescence localized to myocytes above the IgG background fluorescence. Laser settings and exposure times were identical in these two micrographs.

α7nAChR-Activated Signaling Events in Cultured Cardiomyocytes

NRVMs were cultured to study the time course of α7nAChR-initiated activation of intracellular signaling pathways under conditions of hypoxia/reoxygenation and normoxia. Based on preliminary studies using 1×10^{-9}, 10^{-8} and 10^{-7} M GTS21, we determined that 10^{-9} M was optimum for activation of signaling pathways in these cell-based experiments. Quantitation of immunoblot analysis showed that after 8 h of hypoxia, reoxygenation significantly increased phosphorylation of JNK within 10 min, and this effect was abrogated by GTS21 treatment ($p < 0.05$) (Figure 6A). In contrast to the results in perfused hearts, phosphorylation of p38MAPK in NRVM was not altered significantly by

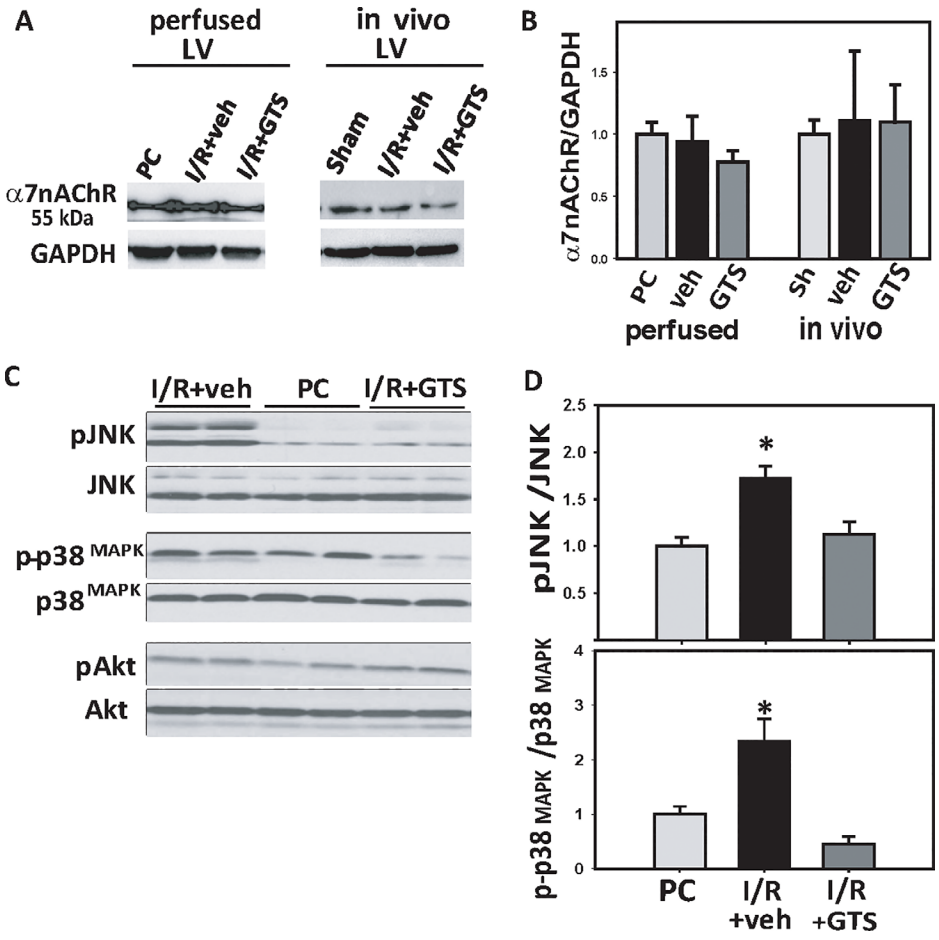

Figure 4. Intracellular signaling pathway activation in isolated perfused rat hearts exposed to I/R. (A) Representative Western blots (WB) showing α7nAChR protein content in rat LV of *in vivo* and *ex vivo* models of I/R injury treated with GTS21 or vehicle; PC, perfusion control; no statistical differences among groups (n = 4–5/group). (B) Quantitation of immunoblots in (A) showing α7nAChR normalized to GAPDH. (C) Representative immunoblots for JNK, $p38^{MAPK}$, AKT and their phosphorylated isoforms in I/R perfused LVs treated with vehicle or GTS21. (D) Quantitation of the WB shown as bar graphs for phospho-JNK to total JNK and p-$p38^{MAPK}$ to total $p38^{MAPK}$ ratios normalized to PC. Values are mean ± SE; *$p < 0.01$ versus all groups. Statistical significance determined by one-way ANOVA.

either reoxygenation or GTS21 treatment (Figure 6B). Rapid phosphorylation of Erk1/2 in response to GTS21 occurred under normoxic conditions (Figure 6D), and although this response was also observed during reoxygenation, it did not reach statistical significance ($p = 0.07$) (Figure 6C). Additional signaling pathways that were interrogated but showed no effect of GTS21 treatment included Akt, AMP-activated kinase, Jak2/Stat3 and DUSP4 (dual-specificity phosphatase) (data not shown).

GTS21 Increases Intracellular ATP Concentration after I/R

Since GTS21 treatment preserved mitochondrial membrane potential and improved contractility early in the reperfusion period, we measured intracellular ATP concentration. AC16 cells were exposed to 6 h hypoxia followed by 1 h reoxygenation (H/R) with or without GTS21 treatment and compared with cells cultured in normoxic conditions. As expected, ATP concentration in cells exposed to H/R decreased by 35% ($p < 0.001$); however, cells treated with GTS21 (10^{-9} M and 10^{-8} M) had significantly higher intracellular ATP, similar to levels measured under normoxic conditions (Figure 7A). Pretreatment with MLA completely blocked this effect of GTS21 (Figure 7B). MLA treatment alone had no effect on cellular ATP content (data not shown).

DISCUSSION

The key finding in this study is that activating nicotinic acetylcholine receptors in the myocardium significantly reduced ischemia reperfusion injury, with improvement in contractile function as a result of a significant reduction in infarct size and preservation of mitochondrial membrane potential, maintenance of intracellular ATP concentration, reduced tissue ROS and inhibition of intracellular stress pathway activation. Secondly, these effects were independent of a systemic inflammatory response, since the *ex vivo* perfused heart preparation that was isolated from peripheral immune and central nervous systems showed an immediate improvement in contractility at the onset of reperfusion in response to treatment with a selective α7nAChR agonist, GTS21. In addition, results from *in vivo* I/R studies showing a significant improvement in all measures of left ventricular function within 1 h of reperfusion following GTS21 treatment suggests that the protective effects of nicotinic receptor activation may be independent of peripheral immune responses to injury. Although other studies have reported that cholinergic receptor stimulation reduced inflammation and/or leukocyte infiltration into sites of ischemic injury in organs including the heart and kidney (3,43,49,51), it remains plausible that the reduced trafficking of leukocytes to sites of injury is secondary to the direct actions of cholinergic receptor-mediated increases in cell survival and function. Yeboah *et al.* (51) showed that renal damage after I/R was similarly reduced in both vagotomized and control animals following nicotine treatment. Calvillo *et al.* (3) showed that vagus nerve

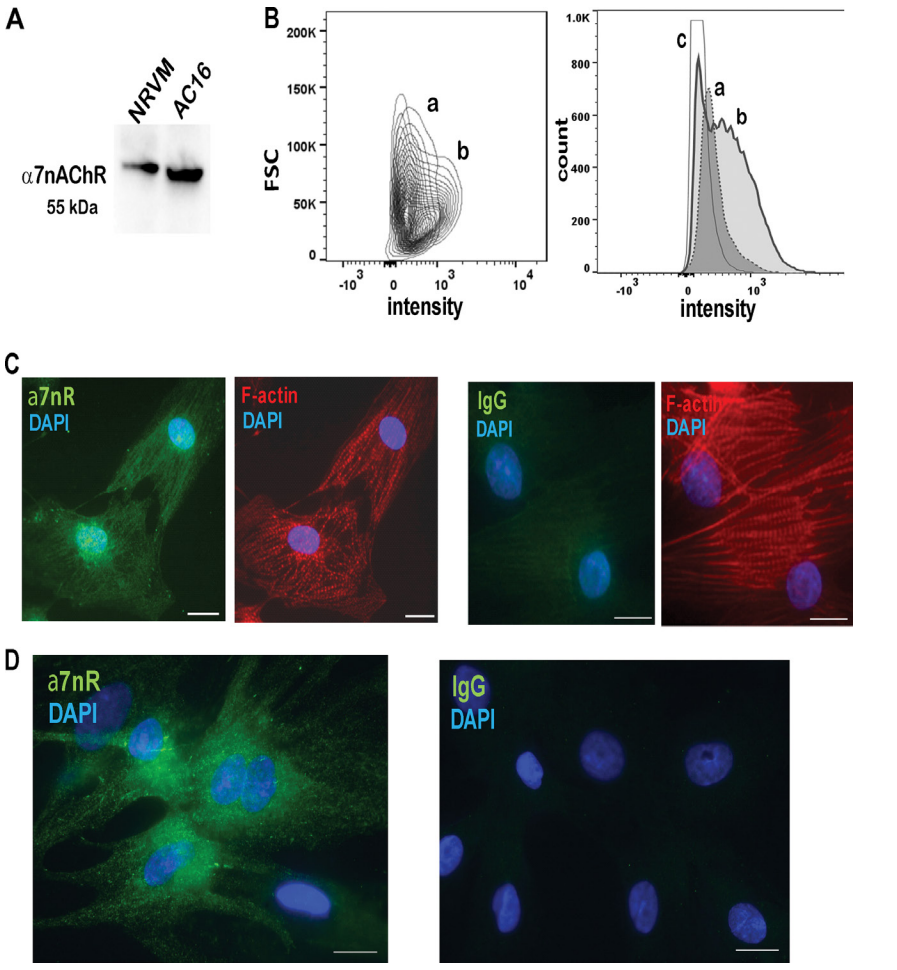

Figure 5. Localization of α7nAChRs in cultured cardiomyocytes. (A) Immunoblot analysis of α7nAChR (55 kDa) in total lysates of neonatal rat ventricular myocytes (NRVM) and adult human cardiomyocytes AC16. (B) FACS analysis of intact AC16 cells sorted by intensity of bound anti-α7nAChR antibody versus forward scatter (FSC). Contour map (*left*) shows distinct populations of cells that are quantified in the histogram (*right*): cells in peak-b are bound with fluorescence-labeled antibody; cells in peak-a were incubated with antibody preadsorbed with peptide immunogen; cells incubated with isotype control IgG are in peak-c. (C) Fluorescence microscopy localized α7nAChR (a7nR) in NRVM using a rabbit anti-α7nAChR antibody and FITC-labeled secondary antibody. Counterstaining with TRITC-labeled phalloidin identified F-actin in cardiomyocytes. Using identical exposure settings, isotype rabbit IgG showed low background fluorescence in myocytes stained for F-actin. Scale bars represent 20 μm. (D) Micrographs taken at the same exposure settings show strong localization of anti-α7nAChR antibodies to NRVMs while the IgG isotype control is weakly fluorescent. Scale bars, 20 μm.

stimulation limited infarct size in an animal model of I/R and, by 24 h, reduced macrophage/neutrophil infiltration at the site of injury. Given that these effects were partially blocked by a nonselective nicotinic receptor antagonist, further suggests that both pharmacologic and neural activation of cholinergic receptors could be cardioprotective.

Delfiner *et al.* (8) and others (1,41) have identified postganglionic cholinergic nerve fibers in the ventricular epicardium that stain with anti–choline acetyltransferase antibody, indicating that these neurons are a local source of acetylcholine. Recent studies have also identified the cardiomyocyte as a nonneuronal source of acetylcholine synthesis and secretion. Acting in an autocrine/paracrine manner, acetylcholine has been reported to limit myocardial tissue injury in ischemia and reduce cardiac remodeling in response to hypertrophic signals (15,36), thus providing a rationale for therapeutic targeting of cholinergic receptors in the heart. We initially focused the present study on the α7 subtype of nAChR due to its central role in mediating the antiinflammatory effects of cholinergic stimulation (38,47) (reviewed in [34]). The presence of α7nAChRs in myocytes and coronary vessels of the heart (10) and published reports localizing these receptors to mitochondria suggest a role beyond an inflammatory one (11,29). Herein, we identified α7nAChRs in rat heart homogenates, in cultured primary neonatal rat ventricular myocytes and in a human cardiomyocyte cell line. We did not observe any changes in myocardial α7nAChR protein expression in response to I/R or with GTS21 treatment in either *ex vivo* or *in vivo* experiments. Studies have suggested that α7nAChR desensitization occurs in response to endogenous ACh that is known to increase in the myocardial interstitium during ischemia (20), so that an allosteric modulator of α7nAChR such as galantamine may augment the effects of endogenous ACh (44,48). Galantamine at higher concentrations also functions to inhibit acetylcholinesterase. These activities may partially explain the positive effects of galantamine on LV function in the perfused I/R hearts, although no additive effects were seen when GTS21 was combined with galantamine. The effects of GTS21 on LV function and cell signaling were blocked by MLA, a selective α7nAChR antagonist, providing further evidence that these responses required α7nAChR activation.

To understand how α7nAChR activation resulted in reduced infarct size and decreased tissue ROS after I/R,

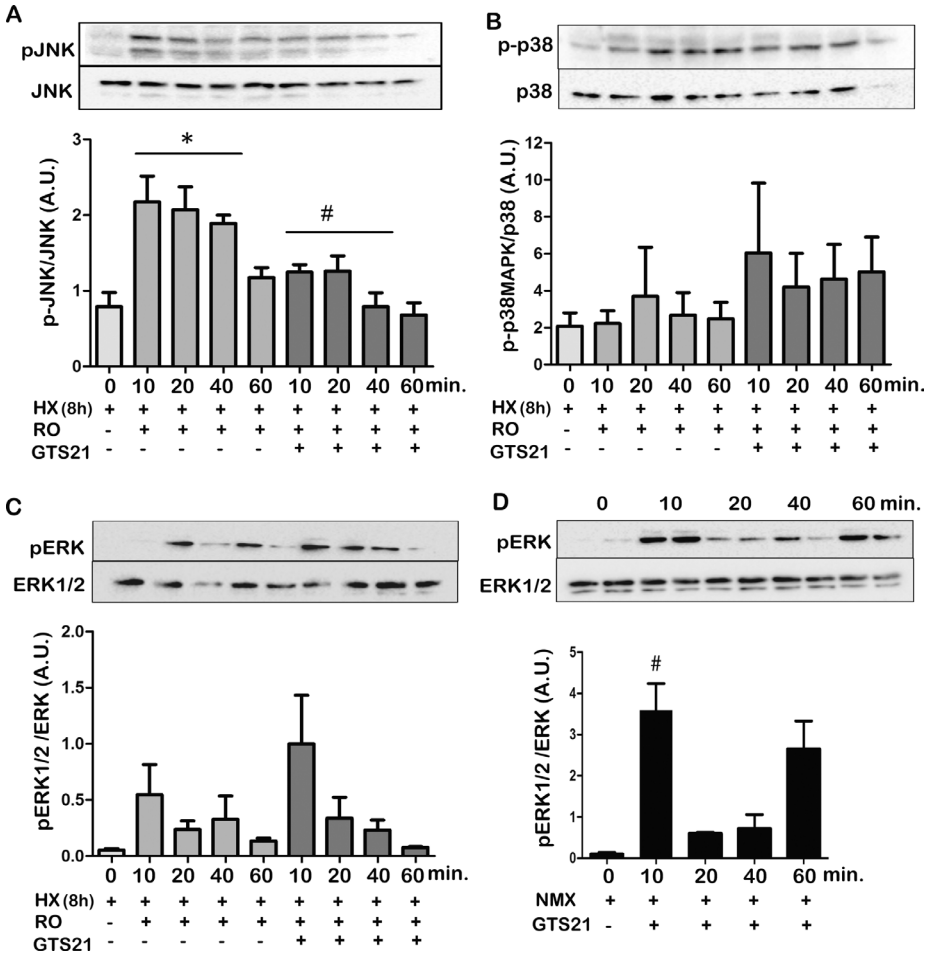

Figure 6. α7nAChR-activated intracellular signaling pathways in cultured cardiomyocytes. NRVM cultures exposed to 8-h hypoxia (HX) followed by reoxygenation (RO) with or without GTS21 (10^{-9} M) treatment; n = 4/time point; Western blots show total and phosphorylated protein kinases. Bar graphs show the quantitation of immunoreactive bands (AU, arbitrary units). (A) ANOVA was used to determine statistical significance among p-JNK/JNK values at 10, 20, 40 min. RO versus HX at 0 min. *$p < 0.01$; two-tailed Student *t* test was used to determine statistical significance between untreated and GTS-treated cells at the same time point $^{\#}p < 0.05$ at 10, 20, 40 min. RO + GTS versus RO at 10, 20, 40 min, respectively. (B) p-p38MAPK to total p38MAPK and (C) pERK1/2 to total Erk1/2. (D) NRVMs under normoxic (NMX) conditions treated with GTS21 showing pERK1/2 /ERK ratios; $^{\#}p < 0.05$ versus (-)GTS at 0 min.

we examined mitochondria that play a critical role in cell death and ROS generation in ischemia (30). We found that the mitochondrial membrane potential was elevated in I/R hearts that would favor ROS formation, and that GTS21 treatment normalized mitochondrial membrane potential. It is interesting to speculate that this effect was mediated by α7nAChRs expressed in mitochondria, as reported Gergalova *et al.* (11), who showed that α7-specific agonists decreased intramitochondrial Ca^{2+} accumulation and cytochrome *c* release after H_2O_2 stimulation. Additionally, these authors showed that α7nAChR co-precipitated with the voltage-dependent anion channel, suggesting a role in mitochondrial permeability transition. To further address the role of mitochondria, we used cultured cells exposed to H/R to mimic cardiac I/R, and, as expected, intracellular ATP concentration was decreased significantly. However, GTS21 treatment during the reoxygenation period normalized ATP content, and this effect was abolished by MLA pretreatment, supporting a α7nAChR-mediated effect.

Several studies have shown that nicotinic receptor activation stimulates cell survival pathways, including PI3K-Akt and ERK1/2 protein kinases, and the Jak/STAT signaling pathway in various cell types, including macrophages and kidney cells (6,46,52). We found that I/R-induced activation of two stress kinase pathways, p38MAPK and JNK, were attenuated by GTS21 treatment, and that phosphorylation of ERK1/2 was increased, similar to mechanisms reported for ACh treatment of cultured cardiomyocytes exposed to hypoxia. These results suggest that agonists of nicotinic receptors may enhance cell survival under hypoxia reoxygenation conditions, either directly or indirectly, by activating intracellular survival pathways. In contrast, other studies using various types of cultured cardiomyocytes support a role of muscarinic receptors in ACh-mediated protective effects during hypoxia including activation of the PI3K/Akt/HIF1α signaling pathways (15), or inhibition of TNFα production and p38MAPK/JNK signaling (27). It is well established that activation of α7nAChRs on macrophages inhibits production and release of TNFα (34,47). Thus the distinct role of nicotinic versus muscarinic receptors on these mechanisms in the heart remains to be determined and is of particular importance should pharmaceuticals targeting specific receptors subtypes be developed to treat myocardial I/R injury. Alternatively, activation of nicotinic receptors localized to coronary vessel endothelial and smooth muscle cells (10,46) may reduce vascular dysfunction after I/R, thus improving perfusion of the myocardium, resulting in preserved contractile function.

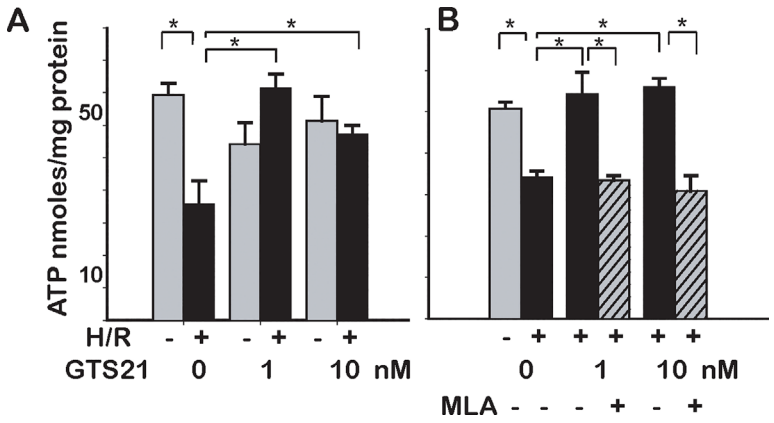

Figure 7. Effects of GTS21 on intracellular ATP. AC16 cells were exposed to 6-h hypoxia followed by 1-h reoxygenation (H/R)(+) or cultured under normoxia (-) conditions. Cellular ATP content was measured using a luciferase assay and normalized to total protein. (A) Cells were treated with GTS21 (1, 10 nM) only during reperfusion. (B) Pretreatment with MLA (100 nM) abolished the GTS21 effect on H/R cells. Data (mean ± SE) represents n = 3–6 cell culture dishes/treatment group. Each ATP assay data point was done in triplicate. Significance was determined by ANOVA post hoc Newman-Keuls; $*p < 0.01$ differences between groups as indicated by the connecting line.

CONCLUSION

In conclusion, our data are consistent with the idea that in a setting of cardiac ischemia reperfusion, activation of α7nAChRs stimulates prosurvival signaling pathways or inhibits stress signals, leading to the preservation of mitochondria, which reduces ROS generation and increases cellular ATP, all of which attenuates tissue injury and improves cardiac contractile function. Furthermore, targeting nicotinic cholinergic receptor pathways by pharmacologic means or neuromodulation has the added benefit of dampening subsequent systemic inflammatory responses in which cytokines released from damaged tissue promote leukocyte trafficking to the site of injury (3, 37,50).

ACKNOWLEDGMENTS

The authors thank Seungjun Ahn, MS (Biostatistics Unit, The Feinstein Institute for Medical Research), for assistance with statistical analysis.

DISCLOSURE

The authors declare that they have no competing interests as defined by *Molecular Medicine*, or other interests that might be perceived to influence the results and discussion reported in this paper.

REFERENCES

1. Batulevicius D, Frese T, Peschke E, Pauza DH, Batuleviciene V. (2013) Remodelling of the intracardiac ganglia in diabetic Goto-Kakizaki rats: an anatomical study. *Cardiovasc. Diabetol.* 12:85.
2. Brodde OE, Bruck H, Leineweber K, Seyfarth T. (2001) Presence, distribution and physiological function of adrenergic and muscarinic receptor subtypes in the human heart. *Basic Res. Cardiol.* 96:528–38.
3. Calvillo L, *et al.* (2011) Vagal stimulation, through its nicotinic action, limits infarct size and the inflammatory response to myocardial ischemia and reperfusion. *J. Cardiovasc. Pharmacol.* 58:500–07.
4. Davidson MM, *et al.* (2005) Novel cell lines derived from adult human ventricular cardiomyocytes. *J. Mol. Cell. Cardiol.* 39:133–47.
5. De Ferrari GM, *et al.* (2011) Chronic vagus nerve stimulation: a new and promising therapeutic approach for chronic heart failure. *Eur. Heart J.* 32:847–55.
6. de Jonge WJ, *et al.* (2005) Stimulation of the vagus nerve attenuates macrophage activation by activating the Jak2-STAT3 signaling pathway. *Nat. Immunol.* 6:844–51.
7. De Meersman RE, Stein PK. (2007) Vagal modulation and aging. *Biol. Psychol.* 74:165–73.
8. Delfiner MS, Siano J, Li Y, Dedkov EI, Zhang Y. (2016) Reduced epicardial vagal nerve density and impaired vagal control in a rat myocardial infarction-heart failure model. *Cardiovasc. Pathol.* 26:21–9.
9. Duprez DA. (2008) Cardiac autonomic imbalance in pre-hypertension and in a family history of hypertension. *J. Am. Coll. Cardiol.* 51:1902–03.
10. Dvorakova M, *et al.* (2005) Developmental changes in the expression of nicotinic acetylcholine receptor alpha-subunits in the rat heart. *Cell Tissue Res.* 319:201–09.
11. Gergalova G, *et al.* (2012) Mitochondria express alpha7 nicotinic acetylcholine receptors to regulate Ca2+ accumulation and cytochrome c release: study on isolated mitochondria. *PloS One.* 7:e31361.
12. Gergalova G, Lykhmus O, Komisarenko S, Skok M. (2014) Alpha7 nicotinic acetylcholine receptors control cytochrome c release from isolated mitochondria through kinase-mediated pathways. *Int. J. Biochem. Cell Biol.* 49:26–31.
13. Handa T, *et al.* (2009) Anti-Alzheimer's drug donepezil markedly improves long-term survival after chronic heart failure in mice. *J. Card. Fail.* 15:805–11.
14. Hausenloy DJ, Yellon DM. (2013) Myocardial ischemia-reperfusion injury: a neglected therapeutic target. *J. Clin. Invest.* 123:92–100.
15. Kakinuma Y, *et al.* (2012) A non-neuronal cardiac cholinergic system plays a protective role in myocardium salvage during ischemic insults. *PLoS One.* 7:e50761.
16. Kakinuma Y, Akiyama T, Sato T. (2009) Cholinoceptive and cholinergic properties of cardiomyocytes involving an amplification mechanism for vagal efferent effects in sparsely innervated ventricular myocardium. *FEBS J.* 276:5111–25.
17. Kakinuma Y, *et al.* (2013) Heart-specific overexpression of choline acetyltransferase gene protects murine heart against ischemia through hypoxia-inducible factor-1alpha-related defense mechanisms. *J. Am. Heart Assoc.* 2:e004887.
18. Katare RG, *et al.* (2009) Vagal nerve stimulation prevents reperfusion injury through inhibition of opening of mitochondrial permeability transition pore independent of the bradycardiac effect. *J. Thorac. Cardiovasc. Surg.* 137:223–31.
19. Katzeff HL, Powell SR, Ojamaa K. (1997) Alterations in cardiac contractility and gene expression during low-T3 syndrome: prevention with T3. *Am. J. Physiol.* 273:E951–6.
20. Kawada T, *et al.* (2000) Differential acetylcholine release mechanisms in the ischemic and non-ischemic myocardium. *J. Mol. Cell. Cardiol.* 32:405–14.
21. Kenessey A, Ojamaa K. (2006) Thyroid hormone stimulates protein synthesis in the cardiomyocyte by activating the Akt-mTOR and p70S6K pathways. *J. Biol. Chem.* 281:20666–72.
22. Khan NS, *et al.* (2015) Cytosolic phospholipase A2alpha is critical for angiotensin II-induced hypertension and associated cardiovascular pathophysiology. *Hypertension.* 65:784–92.
23. Koga K, *et al.* (2011) Macrophage migration inhibitory factor provides cardioprotection during ischemia/reperfusion by reducing oxidative stress. *Antioxid. Redox. Signal.* 14:1191–1202.

24. LaCroix C, Freeling J, Giles A, Wess J, Li YF. (2008) Deficiency of M-2 muscarinic acetylcholine receptors increases susceptibility of ventricular function to chronic adrenergic stress. *Am. J. Physiol.-Heart C.* 294: H810–20.
25. Lara A, *et al.* (2010) Dysautonomia due to reduced cholinergic neurotransmission causes cardiac remodeling and heart failure. *Mol. Cell. Biol.* 30:1746–56.
26. Lataro RM, *et al.* (2013) Increase in parasympathetic tone by pyridostigmine prevents ventricular dysfunction during the onset of heart failure. *Am. J. Physiol. Regul. Integr. Comp. Physiol.* 305:R908–16.
27. Li DL, *et al.* (2011) Acetylcholine inhibits hypoxia-induced tumor necrosis factor-alpha production via regulation of MAPKs phosphorylation in cardiomyocytes. *J. Cell. Physiol.* 226:1052–59.
28. Lin X, *et al.* (2005) Macrophage migration inhibitory factor within the alveolar spaces induces changes in the heart during late experimental sepsis. *Shock.* 24:556–63.
29. Lykhmus O, *et al.* (2014) Mitochondria express several nicotinic acetylcholine receptor subtypes to control various pathways of apoptosis induction. *Int. J. Biochem. Cell. Biol.* 53:246–52.
30. Murphy E, *et al.* (2016) Mitochondrial function, biology, and role in disease: a scientific statement from the American Heart Association. *Circ. Res.* 118:1960–91.
31. Nordstrom P, Religa D, Wimo A, Winblad B, Eriksdotter M. (2013) The use of cholinesterase inhibitors and the risk of myocardial infarction and death: a nationwide cohort study in subjects with Alzheimer's disease. *Eur. Heart J.* 34:2585–91.
32. Okazaki Y, Zheng C, Li M, Sugimachi M. (2010) Effect of the cholinesterase inhibitor donepezil on cardiac remodeling and autonomic balance in rats with heart failure. *J. Physiol. Sci.* 60:67–74.
33. Olshansky B, Sabbah HN, Hauptman PJ, Colucci WS. (2008) Parasympathetic nervous system and heart failure: pathophysiology and potential implications for therapy. *Circulation.* 118:863–71.
34. Pavlov VA, Tracey KJ. (2012) The vagus nerve and the inflammatory reflex—linking immunity and metabolism. *Nat. Rev. Endocrinol.* 8:743–54.
35. Rana OR, *et al.* (2010). Acetylcholine as an age-dependent non-neuronal source in the heart. *Auton. Neurosci-Basic.* 156:82–89.
36. Rocha-Resende C, *et al.* (2012) Non-neuronal cholinergic machinery present in cardiomyocytes offsets hypertrophic signals. *J. Mol. Cell. Cardiol.* 53:206–16.
37. Rocha JA, *et al.* (2016) Increase in cholinergic modulation with pyridostigmine induces anti-inflammatory cell recruitment soon after acute myocardial infarction in rats. *Am. J. Physiol. Regul. Integr. Comp. Physiol.* 310:R697–706.
38. Rosas-Ballina M, *et al.* (2011) Acetylcholine-synthesizing T cells relay neural signals in a vagus nerve circuit. *Science.* 334:98–101.
39. Roy A, *et al.* (2016) Cardiac acetylcholine inhibits ventricular remodeling and dysfunction under pathologic conditions. *FASEB J.* 30:688–701.
40. Roy A, Guatimosim S, Prado VF, Gros R, Prado MAM. (2014) Cholinergic activity as a new target in diseases of the heart. *Mol. Med.* 20:527–37.
41. Rysevaite K, *et al.* (2011) Immunohistochemical characterization of the intrinsic cardiac neural plexus in whole-mount mouse heart preparations. *Heart Rhythm.* 8:731–38.
42. Sabino JP, da Silva CA, de Melo RF, Fazan R Jr, Salgado HC. (2013) The treatment with pyridostigmine improves the cardiocirculatory function in rats with chronic heart failure. *Auton. Neurosci.* 173:58–64.
43. Sadis C, *et al.* (2007) Nicotine protects kidney from renal ischemia/reperfusion injury through the cholinergic anti-inflammatory pathway. *PloS One* 2:e469.
44. Samochocki M, *et al.* (2003) Galantamine is an allosterically potentiating ligand of neuronal nicotinic but not of muscarinic acetylcholine receptors. *J. Pharmacol. Exp. Therap.* 305:1024–36.
45. Schwartz PJ, De Ferrari GM. (2009) Vagal stimulation for heart failure: background and first in-man study. *Heart Rhythm.* 6:S76–81.
46. Smedlund K, Tano JY, Margiotta J, Vazquez G. (2011) Evidence for operation of nicotinic and muscarinic acetylcholine receptor-dependent survival pathways in human coronary artery endothelial cells. *J. Cell. Biochem.* 112:1978–84.
47. Wang H, *et al.* (2003) Nicotinic acetylcholine receptor alpha7 subunit is an essential regulator of inflammation. *Nature.* 421:384–88.
48. Woodruff-Pak DS, Vogel RW 3rd, Wenk GL. (2001) Galantamine: effect on nicotinic receptor binding, acetylcholinesterase inhibition, and learning. *Proc. Nat. Acad. Sci. U.S.A.* 98:2089–94.
49. Xiong J, *et al.* (2012) Postconditioning with alpha7nAChR agonist attenuates systemic inflammatory response to myocardial ischemia—reperfusion injury in rats. *Inflammation.* 35:1357–64.
50. Xiong J, *et al.* (2012) Combined postconditioning with ischemia and alpha7nAChR agonist produces an enhanced protection against rat myocardial ischemia reperfusion injury. *Chin. Med. J. (Engl.)* 125:326–31.
51. Yeboah MM, *et al.* (2008) Cholinergic agonists attenuate renal ischemia-reperfusion injury in rats. *Kidney Int.* 74:62–69.
52. Yeboah MM, Xue X, Javdan M, Susin M, Metz CN. (2008) Nicotinic acetylcholine receptor expression and regulation in the rat kidney after ischemia-reperfusion injury. *Am. J. Physiol. Renal Physiol.* 295: F654–61.
53. Zhang YH, *et al.* (2009) Chronic vagus nerve stimulation improves autonomic control and attenuates systemic inflammation and heart failure progression in a canine high-rate pacing model. *Circ-Heart Fail.* 2:692–99.

Cite this article as: Mavropoulos SA, *et al.* (2017) Nicotinic acetylcholine receptor–mediated protection of the rat heart exposed to ischemia reperfusion. *Mol. Med.* 23:120–33.